NASA Technical Memorandum 105288

Development of a Steady Potential Solver for Use With Linearized, Unsteady Aerodynamic Analyses

Daniel Hoyniak
Lewis Research Center
Cleveland, Ohio

and

Joseph M. Verdon
United Technologies Research Center
East Hartford, Connecticut

Prepared for the
Sixth International Symposium on Unsteady Aerodynamics, Aeroacoustics, and Aeroelasticity of Turbomachines and Propellers
sponsored by the International Union for Theoretical and Applied Mechanics
Notre Dame, Indiana, September 15–19, 1991

NASA

DEVELOPMENT OF A STEADY POTENTIAL SOLVER FOR USE WITH LINEARIZED, UNSTEADY AERODYNAMIC ANALYSES

Daniel Hoyniak
National Aeronautics and Space Administration
Lewis Research Center
Cleveland, Ohio 44135

and

Joseph M. Verdon
United Technologies Research Center
East Hartford, Connecticut

SUMMARY

A full potential steady flow solver (SFLOW) developed explicitly for use with an inviscid unsteady aerodynamic analysis (LINFLO) is described herein. The steady solver uses the non-conservative form of the nonlinear potential flow equations together with an implicit, least-squares, finite-difference approximation to solve for the steady flow field. The difference equations were developed on a composite mesh which consists of a C–grid embedded in a rectilinear (H–grid) cascade mesh. The composite mesh is capable of resolving blade-to-blade and far-field phenomena on the H–grid, while accurately resolving local phenomena on the C–grid. The resulting system of algebraic equations is arranged in matrix form using a sparse matrix package and solved by Newton's method.

Steady and unsteady results are presented for two cascade configurations: a high-speed compressor and a turbine with high exit Mach number.

INTRODUCTION

The need for accurate and numerically efficient techniques for predicting the aeroelastic and aeroacoustic response behavior of turbomachinery blading has resulted in the development of inviscid unsteady aerodynamic linearization procedures (see Atassi & Akai, 1980; Whitehead, 1982; Verdon & Caspar, 1982, 1984; Hall & Clark, 1991; and Caruthers and Dalton, 1991). In general these techniques address the unsteady response of an isolated, two-dimensional cascade. They include the effects of realistic design features such as blade geometry, mean blade loading, and operation at transonic Mach numbers. The unsteady fluctuations are regarded as small-amplitude harmonic (in time) disturbances superimposed on a fully nonuniform mean or steady flow. The steady flow is determined as a solution of the nonlinear inviscid equations, while the unsteady flow is governed by linear equations with variable coefficients that depend on the underlying steady flow. Thus, in order to predict the unsteady response, it is first necessary to determine the steady flow field.

Recently, several investigators have used Newton's method to obtain solutions to the equations of fluid dynamics. Giles (1985) and Hall & Crawley (1989) used the Euler equations to solve for the transonic flow through a two-dimensional cascade of airfoils. Bender & Khosla (1988) and Bailey & Beam (1991) both used this technique to obtained solutions of the two-dimensional inviscid and viscous equations associated with flow over an isolated airfoil.

This paper describes the application of Newton's method to the solution of the nonlinear, steady potential equation describing the flow through a two-dimensional cascade of airfoils. The resulting computer algorithm is called SFLOW. Newton's method was selected for two reasons: First, the solution of the nonlinear velocity potential equation is obtained from a series of linear equations that are similar to those obtained for the linearized unsteady problem. Thus, the numerical algorithm developed for the solution of the linearized unsteady equation can be used in the solution of the nonlinear steady equation. Second, this method has the potential for obtaining a converged solution very quickly.

The first section of the paper describes the partial differential equation and boundary conditions for the nonlinear steady velocity potential. Next, Newton's method is applied and the resulting linear differential equation and boundary conditions are related to those obtained for the linearized unsteady flow. The last section describes the application of the SFLOW algorithm, together with the linearized inviscid unsteady analysis (LINFLO) of Verdon and Caspar (1984, 1987), to the solution of the steady and unsteady flows associated with a high-speed compressor cascade and the turbine cascade designated as the fourth standard configuration by Bölcs & Fransson (1986).

GOVERNING EQUATIONS

The cascade geometry used in this mathematical model is shown in figure 1. It consists of an isolated, infinite array of identical airfoils. The reference airfoil for the cascade defines the origin of a Cartesian coordinate system with the ξ axis oriented along the cascade axial direction, and the η axis oriented along the tangential direction. The gap distance between blades is defined by the magnitude of the gap vector $\vec{G}$ which is directed along the η axis. The inlet and exit flow angles are defined by, $\Omega_{\mp\infty}$, respectively. The steady-state positions of the airfoil chord lines coincide with the line segments $0 \le \xi \le \cos\Theta$, $\eta = \xi \tan\theta + mG$, where m is a blade index number and $m = 0$ denotes the reference blade and where θ is the cascade stagger angle. The blade and cascade physical parameters have been normalized by the blade chord.

FIELD EQUATIONS

The equations that govern the steady, two-dimensional, adiabatic flow, with negligible body forces, of an inviscid non-heat-conducting perfect gas are obtained from the conservation of mass, momentum, and energy. It is also assumed that at some distance upstream ($\xi < \xi_{-\infty}$) and downstream ($\xi > \xi_{+\infty}$) the flow is at most a small isentropic and irrotational perturbation to the steady uniform flow. Because of these assumptions the flow is isentropic and irrotational throughout the domain, and the velocity field can be defined in terms of a velocity potential function. The steady flow field can now be defined by the conservation of mass equation,

$$\nabla \cdot \left(\tilde{\rho}\nabla\tilde{\Phi}\right) = 0 \tag{1}$$

where $\tilde{\rho}$ is the density and $\tilde{\Phi}$ is the velocity potential. In addition to this mass conservation equation, the following relationships between the mean flow variables can be obtained from the momentum equation

$$\tilde{\rho}^{\gamma-1} = \left\{M_{-\infty}\tilde{A}\right\}^2 = 1 - \left(\frac{\gamma-1}{2}\right)M_{-\infty}^2\left\{(\nabla\tilde{\Phi})^2 - 1\right\} \tag{2}$$

where $\tilde{A}$ is the local speed of sound propagation and $M_{-\infty}$ is the inlet Mach number. Equations (1) and (2) can be combined to determine a single nonconservative equation for the potential, that is,

$$\tilde{A}\,\nabla^2\tilde{\Phi} - \nabla\tilde{\Phi}\cdot\frac{\nabla(\nabla\tilde{\Phi})^2}{2} = 0 \tag{3}$$

BOUNDARY CONDITIONS

In addition to the field equation (eq. (3)), the flow is subject to the following boundary conditions in order to obtain a solution for the steady flow field. If we assume that the flow remains attached to the blade surfaces, the velocity potential must satisfy the flow tangency condition

$$\nabla\tilde{\Phi}\cdot\vec{n} = 0 \qquad \vec{X} \in B_m \tag{4}$$

where $\vec{n}$ is a unit normal vector to the airfoil surface, $\vec{X}$ is a position vector, and B_m refers to the m^{th} blade surface.

For the steady flows being considered here, the inlet and exit velocities are subsonic. The inlet and exit boundary conditions require that three of the four uniform free-stream components (e.g., $V_{\pm\infty}$ or $\Omega_{\pm\infty}$) be specified. The fourth is determined so that the global form of the mass conservation is satisfied. In addition, conditions can be imposed at the blade edges (e.g., a zero load condition at a sharp trailing edge (Kutta condition)). In this case, the flow at the trailing edge of the airfoil must satisfy the following relationship:

$$\left|\frac{\partial\tilde{\Phi}^{+}_{\text{TE}}}{\partial S^{+}}\right| = \left|\frac{\partial\tilde{\Phi}^{-}_{\text{TE}}}{\partial S^{-}}\right| \tag{5}$$

where $S^{\pm}$ is the arc distance along the upper (+) and lower (−) surface of the airfoil.

Since the airfoils in this cascade are assumed to be identical and since the inlet flow is uniform, the following blade-to-blade periodicity condition can be applied: Along the upstream periodic boundary

$$\tilde{\Phi}(\xi,\eta + G) - \tilde{\Phi}(\xi,\eta) = V_{-\infty}\sin\Omega_{-\infty}G \tag{6}$$

and along the downstream periodic boundary

$$\tilde{\Phi}(\xi,\eta + G) - \tilde{\Phi}(\xi,\eta) = V_{+\infty} \sin \Omega_{+\infty} G \tag{7}$$

The locations of these periodic boundaries are arbitrary, however, in this model the upstream periodic boundary is chosen so that it is parallel to the inlet velocity vector and intersects the airfoil at the leading edge point. The downstream periodic boundary is arbitrarily chosen. Upon completion of the steady flow calculation, the downstream stagnation streamline is determined since this will be required for the unsteady analysis.

These boundary conditions allow the steady flow to be calculated in a region represented by a single extended flow passage. This region is defined by the upstream and downstream periodic boundaries, the upstream and downstream far-field boundaries, the upper surface of the reference airfoil ($m = 0$), and the lower surface of the airfoil defined by $m = 1$.

NEWTON'S METHOD

The velocity potential may be rewritten as

$$\tilde{\Phi}(\vec{X}) = \Phi(\vec{X}) + \phi(\vec{X}) \tag{8}$$

where Φ is an approximation to the solution $\tilde{\Phi}$, where $\phi = \tilde{\Phi} - \Phi$ is a correction term, and where $\vec{X}$ is a position vector. After substituting equation (8) into (3) and performing the necessary algebra we find that

$$A^2 \nabla^2 \phi - (\gamma - 1) \nabla^2 \Phi \frac{\bar{D}\phi}{Dt} - \frac{\bar{D}^2 \phi}{Dt^2} - \nabla\phi \cdot \frac{\nabla(\nabla\Phi)^2}{2} = - A^2 \nabla^2 \Phi + \nabla\Phi \cdot \frac{\nabla(\nabla\Phi)^2}{2} \tag{9}$$

where the material derivative operator is defined as

$$\frac{\bar{D}}{Dt} = \nabla\Phi \cdot \nabla \tag{10}$$

and where

$$A^2 = 1 - \left(\frac{\gamma-1}{2}\right) M_{-\infty}^2 \left[(\nabla\Phi)^2 - 1\right] \tag{11}$$

Equation (9) can be written in the form

$$L(\Phi)\phi = N(\Phi) \tag{12}$$

where L is a linear differential operator, which depends on the steady velocity potential, Φ, and N is a nonlinear differential operator that also depends on Φ. The initial distribution for Φ is some estimate of the converged solution, e.g., $\Phi^0 = \vec{V}_{-\infty}\xi$. The solution to equation (9) then proceeds as follows: At the n^{th} Newton iteration equation (9) is solved for the correction ϕ^n using the estimate of the converged solution Φ^n. The $(n+1)^{th}$ (i.e., Φ^{n+1}) approximation to $\tilde{\Phi}$ becomes $\Phi^{n+1} = \Phi^n + \phi^n$. This process is continued until $|\phi^n| < \varepsilon_{max}$, where ε_{max} is some preselected convergence tolerance.

In addition to rewriting the field equation into a form that will facilitate the application of Newton's method, it is also necessary to convert the boundary conditions to this form. This is accomplished by substituting equation (8) into the boundary conditions equations (5) to (8) and performing the necessary algebra. The resulting expressions are

for flow tangency

$$\nabla\phi \cdot \vec{n} = -\nabla\Phi \cdot \vec{n} \tag{13}$$

for periodicity

$$\phi(\xi,\eta + G) - \phi(\xi,\eta) = V_{\pm\infty} \sin \Omega_{\pm\infty} G - \left[\Phi(\xi,\eta + G) - \Phi(\xi,\eta)\right] \tag{14}$$

and for the Kutta condition

$$\left|\frac{\partial\phi^+_{TE}}{\partial S^+}\right| - \left|\frac{\partial\phi^-_{TE}}{\partial S^-}\right| = -\left(\left|\frac{\partial\Phi^+_{TE}}{\partial S^+}\right| - \left|\frac{\partial\Phi^-_{TE}}{\partial S^-}\right|\right) \tag{15}$$

The differential equation for the linearized unsteady potential is

$$A^2\nabla^2\phi - (\gamma - 1)\nabla^2\Phi\frac{\bar{D}\phi}{Dt} - \frac{\bar{D}^2\phi}{Dt^2} - \nabla\phi \cdot \frac{\nabla(\nabla\Phi)^2}{2} = 0 \tag{16}$$

where

$$\frac{\bar{D}}{Dt} = i\omega + \nabla\Phi \cdot \nabla \tag{17}$$

A detailed derivation of this equation is given by Verdon & Caspar (1982, 1984). The only difference between the left hand sides of equations (9) and (16) is that the unsteady potential, ϕ, is a complex value. If the blade oscillation frequency, ω, is set to zero in equation (17), the left hand sides of the two expressions are identical. The advantage of using the forms for the field equation and boundary conditions given by equation (9) and equations (13) to (15), respectively, is that the differencing schemes and matrix inversion procedure used in the numerical algorithm for the linearized unsteady potential flow can, with little modification, be used to determine the steady potential flow field. However, since the steady problem is nonlinear, an iterative solution, such as that outlined above, is

needed. Once the steady flow has been determined, the linearized unsteady potential equation can be solved for the unsteady velocity potential and ultimately for the unsteady pressures and global unsteady air loads.

The difference approximations to the linear operator in equation (9) are obtained using an implicit, least-squares, interpolation procedure. This leads to a nine-point "centered" difference stencil at field points within the solution domain and a nine-point one-sided difference stencil at blade surface points. A detailed description of this differencing approximation can be found in Caspar & Verdon (1981).

COMPOSITE CALCULATION MESH

Following Usab & Verdon (1989), the difference approximations are applied on a computational mesh consisting of a sheared H type mesh, which will capture aerodynamic phenomena over the extended blade-passage solution domain, and a local surface-fitted C–mesh, which will resolve high gradient phenomena in the region of blunt leading edges. Details of this composite mesh construction can be found in Usab & Verdon (1989), while details on the construction of the global and local meshes can be found in Caspar & Verdon (1981). Only a brief outline of the composite mesh procedure will be given here.

The composite mesh used in this model is constructed by overlaying the local surface fitted mesh over the global cascade mesh (fig. 2). Points on the composite mesh can be identified as cascade-mesh solution points, local-mesh solution points, cascade-mesh coupling points, and local-mesh coupling points, depending on where they lie with respect to a user-defined overlap zone. The overlap region is defined in terms of the local mesh by stepping in n cells from the outer boundary of the local mesh. Composite mesh points are identified as cascade-mesh solution points if they lie outside the interior boundary of the overlap zone, and cascade-mesh coupling points if they are needed to complete the differencing stencil for cascade-mesh solution points lying within the overlap zone. Local-mesh solution points are those which lie inside the outer boundary of the local mesh. While local-mesh coupling points are those that lie on the outer boundary of the local mesh.

The inclusion of these coupling points into the system of discrete equations destroys the block tridiagonal structure that exists when the H–grid and C–grid are considered separately. Although each coupling equation involves points that are spatially close to the coupling point under consideration, they are not necessarily neighbors in the composite equation system. Therefore, the final system of equations contains a sparse coefficient matrix of large band width. Consequently, special storage and inversion techniques are required to achieve an efficient solution. The sparse matrix solver used is that developed by Eisenstat et al. (1977).

MODEL VERIFICATION

The mathematical model for the steady flow calculation was verified using two cascade configurations. Composite-mesh steady flow solutions were determined for both cascades. In both cases converged solutions were obtained in six or less iterations. Once the steady calculations were obtained, the linearized unsteady aerodynamic model, LINFLO, developed by Verdon & Caspar (1982, 1984) was used to calculate the unsteady response of the cascade to a prescribed blade motion.

NACA 0006

The first geometry chosen was one studied by Usab & Verdon (1990). The blades are constructed by superposing the thickness distribution of a modified NACA four-digit series airfoil on a circular-arc camber line. The cascade geometry has a solidity of unity (i.e., $G = 1.0$), and a stagger angle, Θ, of 45°. The inlet Mach number, $M_{-\infty}$, was set at 0.7, and the inlet flow angle, $\Omega_{-\infty}$, was 55°. The steady flow is assumed to satisfy a Kutta condition at the trailing edge; therefore, only the inlet Mach number and flow angle were specified.

The composite mesh used to calculate the steady flow through this cascade geometry is shown in figure 2. It is made up of a global H–mesh consisting of 96 axial and 21 tangential lines. The local C–mesh consists of 71 radial and 21 circumferential lines. The predicted blade surface Mach number distribution for this mesh is shown in figure 3. Also shown is a prediction obtained from the steady velocity potential model, CASPOF, developed by Caspar, Hobbs, & Davis (1980). It should be noted that CASPOF also uses both a global H–mesh and a local C–mesh; however, the two meshes do not overlap, and the governing equations are not solved simultaneously on both meshes as it is in the present analysis. In the CASPOF prediction the H–mesh was used to obtain a global solution that then provided the outer boundary condition for the C–mesh calculation. The exit Mach number, $M_{+\infty}$, and flow angle, $\Omega_{+\infty}$, calculated by the present method were 0.447° and 40.3° respectively. Those obtained from CASPOF were $M_{+\infty} = 0.446°$ and $\Omega_{+\infty} = 40.2°$. Figure 3 also displays the agreement between the two predictions. The small differences in the leading and trailing edge regions are attributed to the differences in the meshes and the solution techniques used in both models.

Having obtained a steady solution, an unsteady calculation was made to demonstrate the coupling to the unsteady flow solver. The LINFLO code was used to calculate the unsteady blade surface pressures resulting from a harmonic torsion mode oscillation of the blades. The reduced frequency of the blade motion based on chord is unity, and the elastic axis is placed at midchord. Motions at two interblade phase angles are considered such that one corresponds to a subresonant motion, and the other to a superresonant motion. Figure 4 shows the real and imaginary components of the predicted unsteady pressure as a function of blade chord for $\sigma = 180°$ (subresonant motion) and $\sigma = 30°$ (superresonant motion). Also shown is the prediction from LINFLO using the steady results obtained from CASPOF. As can be seen the two predictions agree quite well, the small differences in the leading and trailing edge regions being attributed to the noted differences in the two steady predictions.

TURBINE CASCADE

The second test case selected for the verification of the steady flow solver is a turbine cascade, the fourth standard configuration reported by Bölcs and Fransson (1986). In the present study, the airfoil geometry was modified so that the profile closed in a wedge-shaped trailing edge. This modification was done in such a manner that the chord of the blade was not changed. The cascade geometry consists of a set of airfoils that have a stagger angle, Θ, of 56.6° and a blade spacing G of 0.76. Once the steady flow solution is obtained, the unsteady aerodynamic response at the blade surface resulting from a prescribed blade motion can be determined using the LINFLO code.

Bölcs & Fransson (1986) and He (1989) both report that, in order to match the experimentally determined exit conditions, the effect of streamtube height variation needs to be included in the steady flow calculations. He (1989) used a linear variation with an exit height to inlet height ratio of 1.1. Since the steady flow model used is this report does not presently have this capability, the steady flow

calculations were performed by matching the experimentally determined exit Mach number ($M_{+\infty}$ = 0.90). A comparison of the predicted blade surface Mach number distribution with the experimental data for this exit condition is shown in figure 5. The inlet Mach number was determined to be 0.26, the inlet flow angle, 45°, and the exit flow angle, 71.8°. The experimentally determined exit flow angle was 71.0°. Figure 5 shows the agreement between the prediction and data to be quite good from the leading edge to about 85 percent chord. The discrepancies over the last 15 percent of the blade is probably related to the blade modification, and the constant streamtube height used in the calculation.

Unsteady response predictions for a translational motion with displacement amplitudes of $h_x = 0.0016$ and $h_y = 0.0029$ in the x and y directions, a reduced frequency based on a chord of 0.24, and oscillation at an interblade phase angle, σ, of $-90°$ is shown in figure 6. This figure shows the magnitude and phase of the unsteady pressure on the suction and pressure surfaces of the reference airfoil as a function of chordwise distance. There is reasonable agreement between the prediction and experiment for the magnitude of the unsteady response on the suction surface. The pressure surface comparison shows good agreement except in the leading-edge region. The comparison of the phase information shows that the experimental trend on the pressure surface is well predicted while that on the suction surface is not predicted in the trailing-edge region. The oscillations observed in the predictions can be related to the blade surface definition.

Figure 7 shows a plot of the aerodynamic damping, Ξ, versus interblade phase angle. The calculated values of aerodynamic damping are in reasonable agreement with the measured values for $\sigma = 0°$ and 180°, but wide discrepancies exist for $\sigma = \pm 90°$. These discrepancies are probably related to the noted differences between the predicted and measured steady behavior in the trailing-edge region of the blade.

CONCLUDING REMARKS

The steady potential analysis (SFLOW) described in this paper has resulted in two improvements in the ability to calculate the steady potential field of a two-dimensional cascade. The first is the implementation of a composite mesh solution procedure which allows detailed flow information to be obtained in the vicinity of blunt leading edges. The second is the use of Newton's method for the solution of a nonlinear equation. This results in a numerical procedure that converges rapidly. The coupling of this solver to an existing linearized unsteady solver results is a computationally efficient model that can be used to study the aeroelastic and aeroacoustic behavior of advanced turbomachinery configurations.

The steady portion of the model has been verified by comparison with other predictions for a compressor cascade and with experimental data for a turbine cascade. The results have been used as input data for the linearized unsteady analysis. In the case of compressor geometry, the steady calculation agrees quite well with predictions made using another steady flow solver. The steady predictions for the turbine geometry showed good agreement with the experimental results of Bölcs & Fransson (1986) despite the fact that no stream tube height variation was assumed in the steady solver. In general, the unsteady predictions for the turbine are in good agreement with the data for both the magnitude and phase of the unsteady pressure response on the pressure surface of the airfoil. However, although the suction surface predictions showed reasonable agreement for the magnitude of the unsteady pressure, the predictions and measurements for the phase are in poor agreement. The aerodynamic damping prediction were in agreement with the measurements for interblade phase angles of $\pm 180°$, but wide discrepancies exists for $\sigma = \pm 90°$.

REFERENCES

Atassi, H., and Akai, T.J. 1980. "Aerodynamic and Aeroelastic Characteristics of Oscillating Loaded Cascades at Low Mach Number. I Pressure Distribution, Forces and Moments," *J. Eng. Power*, vol. 102, no. 2, pp. 344–351.

Bailey, H.E., and Beam, R.M. 1991. "Newton's Method Applied to Finite-Difference Approximations for the Steady-State Compressible Navier-Stokes Equations," *J. Comput. Phys.*, vol. 93., pp. 108–127.

Bender, E.E., and Khosla, P.K. 1988. "Application of Sparse Matrix Solvers and Newton's Method to Fluid Flow Problems," AIAA Paper 88-3700–CP.

Bölcs, A., and Fransson, T.H. 1986. "Aeroelasticity in Turbomachines—Comparison of Theoretical and Experimental Cascade Results," AFOSR-TR-87-0687 (avail. NTIS, AD-A181763).

Caruthers, J.E., and Dalton, W.N. 1991. "Unsteady Aerodynamic Response of a Cascade to Nonuniform Inflow," ASME Paper 91-GT-174.

Caspar, J.R., Hobbs, D.E., and Davis, R.L. 1980. "Calculation of Two-Dimensional Potential Cascade Flow Using Finite Area Methods," *AIAA J.*, vol. 18, pp. 103–109.

Caspar, J.R., and Verdon, J.M. 1981. "Numerical Treatment of Unsteady Subsonic Flow Past an Oscillating Cascade," *AIAA J.*, vol. 19, pp 1531–1539.

Eisenstat, S.C., Grusky, M.C., Schultz, M.H., and Sherman, A.H. 1977. "The Yale Sparse Matrix Package. II. The Non-symmetric Codes," Research Report no. 114, Yale University, Department of Computer Science, New Haven, CT.

Giles, M. 1985. "Newton Solution of Steady Two-Dimensional Transonic flows," Ph.D. thesis, Massachusetts Institute of Technology.

Hall, K.C., and Clark W.S. 1991. "Prediction of Unsteady Aerodynamic Loads in Cascades Using the Time Linearized Euler Equations on Deforming Grids," AIAA Paper 91–3378.

Hall, K.C., and Crawley, E.F. 1989. "Calculations of Unsteady Flows in Turbomachinery Using The Linearized Euler Equations," *AIAA J.*, vol. 27, no. 6, pp. 777–787.

He, L. 1990. "An Euler Solution for Unsteady Flows Around Oscillating Blades," ASME, *J. Turbomach.*, vol. 112, no. 4, pp. 714–722.

Verdon, J.M., and Caspar, J.R. 1982. "Development of a Linear Unsteady Aerodynamic Analysis for Finite-Deflection Subsonic Cascades," *AIAA J.*, vol. 20, pp. 1259–1267.

Verdon, J.M., and Caspar, J.R. 1984. "A Linearized Unsteady Aerodynamic Analysis for Transonic Cascades," *J. Fluid Mech.*, vol. 149, pp. 403–429.

Whitehead, D.S. 1982. "The Calculation of Steady and Unsteady Transonic Flows in Cascades," Cambridge University Engineering Dept. Rept. CUED/A-Turbo/TR 118, Cambridge, UK.

Usab, W.J., and Verdon, J.M. 1989. "Advances in the Numerical Analysis of Linearized Unsteady Cascades Flows," ASME Paper 90-GT-11.

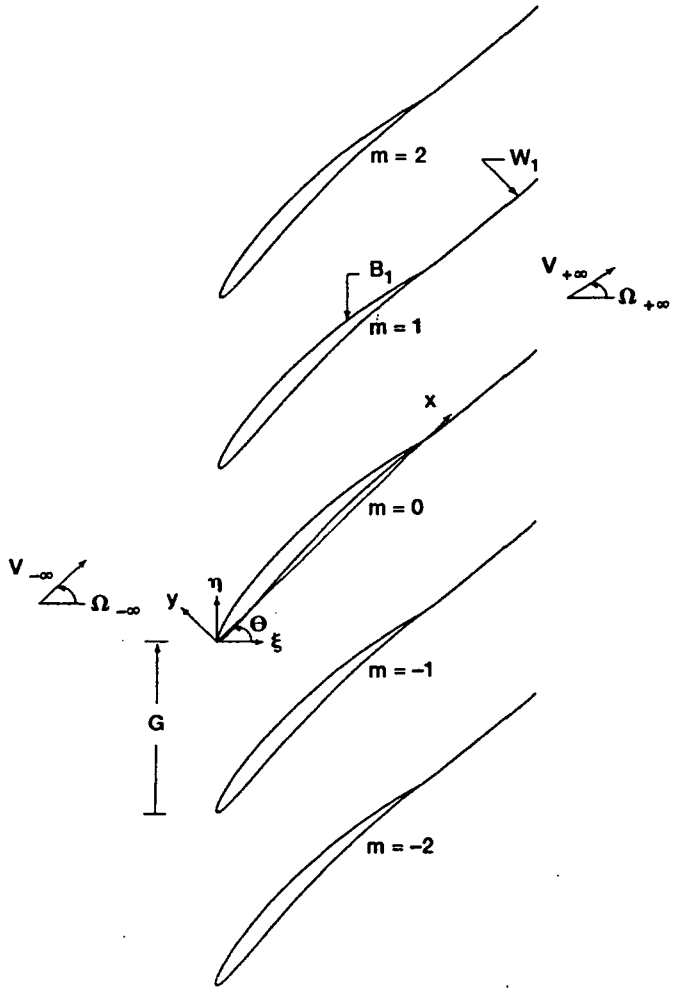

Figure 1.—Two-dimensional compressor cascade; $M_{+\infty} < M_{-\infty} < 1$.

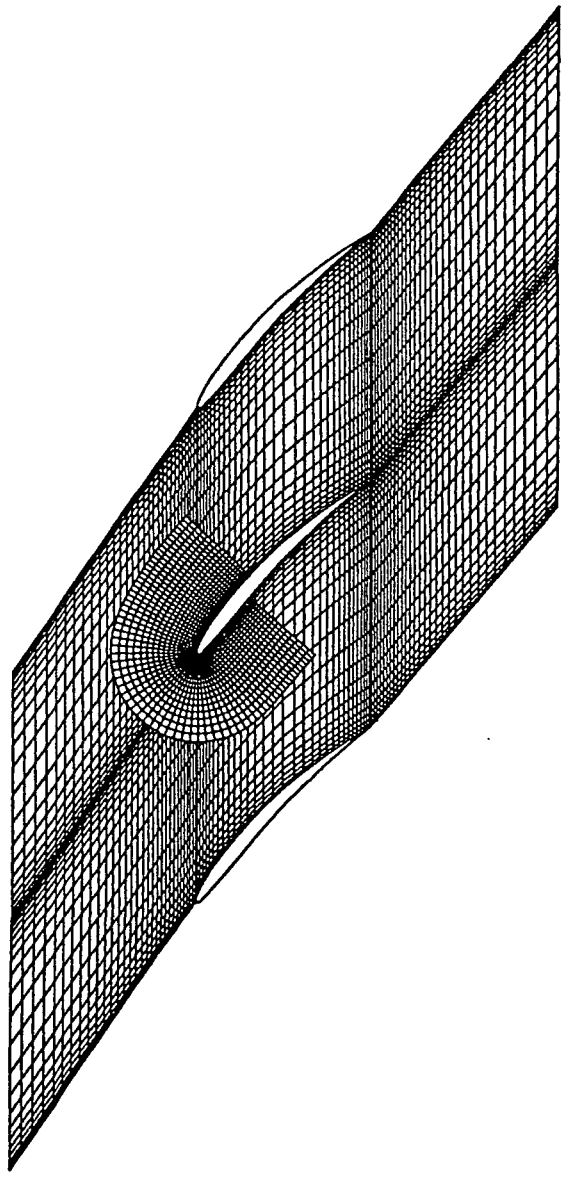

Figure 2.—Composite mesh for NACA 0006 compressor cascade.

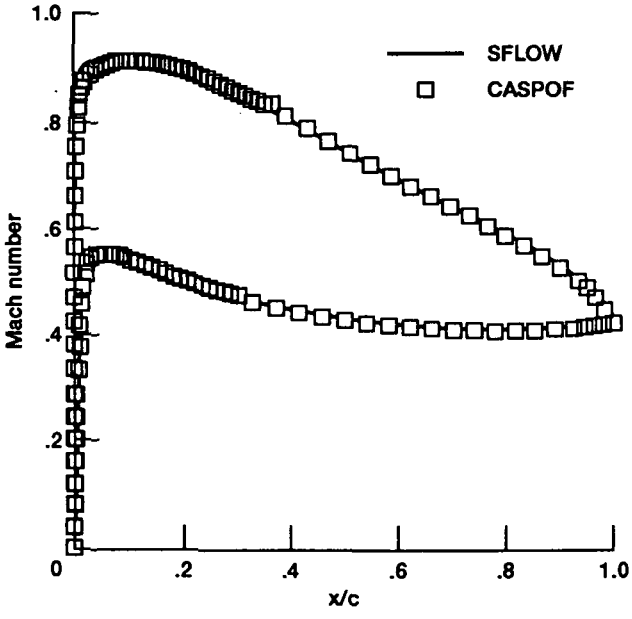

Figure 3.—Steady surface Mach number distribution for NACA 0006 compressor cascade. Inlet Mach number, 0.7; inlet flow angle, 45°.

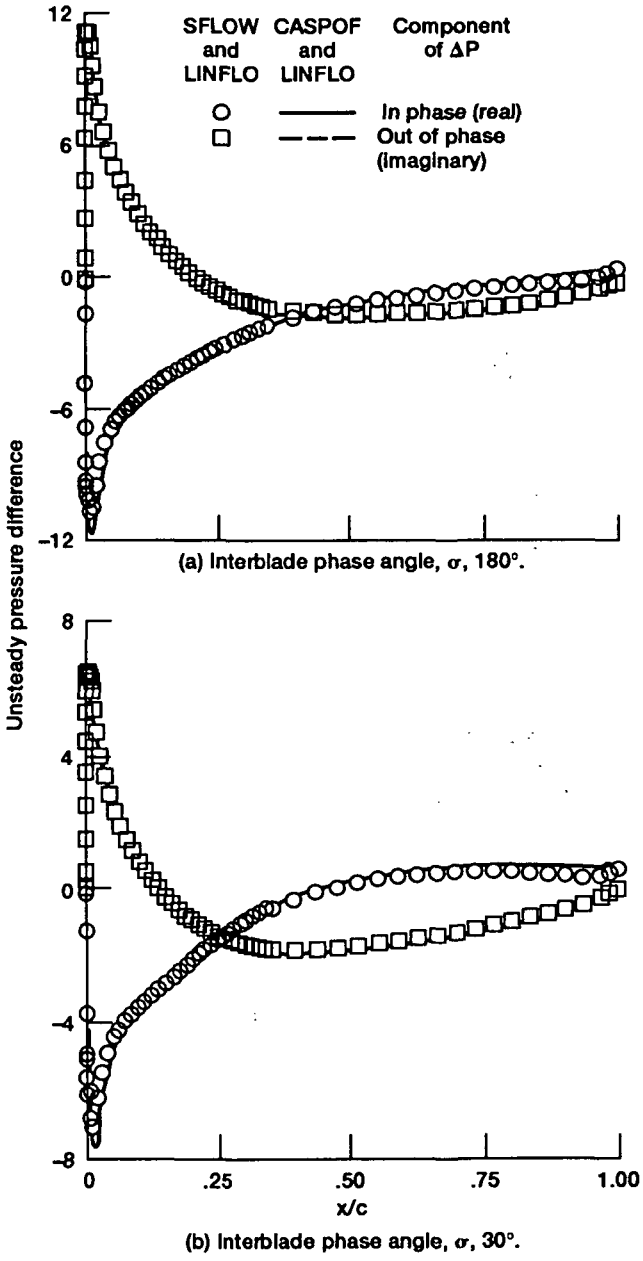

Figure 4.—Unsteady aerodynamic response to torsion mode oscillation of the NACA 0006 cascade, $\alpha = (1,0)$, $\omega = 1$.

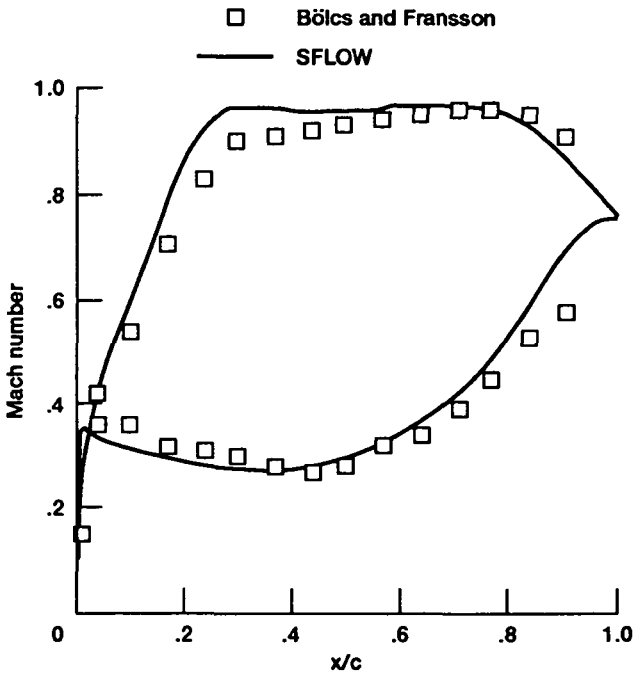

Figure 5.—Steady surface Mach number distribution for turbine cascade. Inlet Mach number, $M_{-\infty}$, 0.26; inlet flow angle, $\Omega_{-\infty}$, 45.

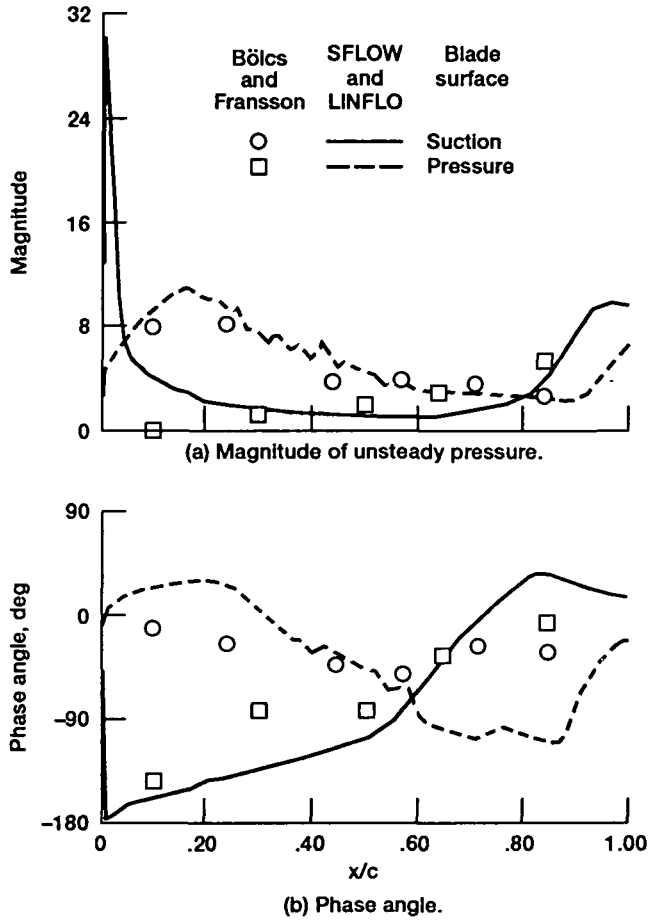

Figure 6.—Unsteady aerodynamic response to bending displacement of turbine cascade. Displacement amplitude, h, (0.0016, 0.0029); blade oscillation frequency, ω, 0.24; interblade phase angle, σ, -90°.

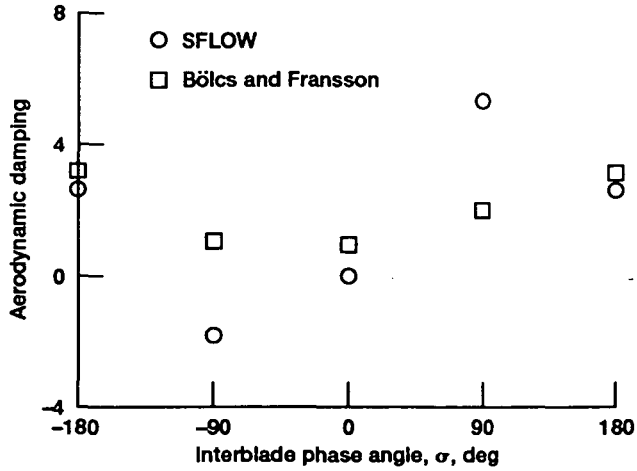

Figure 7.—Aerodynamic damping versus interblade phase angle for turbine cascade.

REPORT DOCUMENTATION PAGE

Form Approved
OMB No. 0704-0188

1. AGENCY USE ONLY (*Leave blank*)	2. REPORT DATE	3. REPORT TYPE AND DATES COVERED
	1991	Technical Memorandum

4. TITLE AND SUBTITLE

Development of a Steady Potential Solver for Use With Linearized, Unsteady Aerodynamic Analysis

5. FUNDING NUMBERS

WU-505-62-10

6. AUTHOR(S)

Daniel Hoyniak and Joseph M. Verdon

7. PERFORMING ORGANIZATION NAME(S) AND ADDRESS(ES)

National Aeronautics and Space Administration
Lewis Research Center
Cleveland, Ohio 44135-3191

8. PERFORMING ORGANIZATION REPORT NUMBER

E-6620

9. SPONSORING/MONITORING AGENCY NAMES(S) AND ADDRESS(ES)

National Aeronautics and Space Administration
Washington, D.C. 20546-0001

10. SPONSORING/MONITORING AGENCY REPORT NUMBER

NASA TM-105288

11. SUPPLEMENTARY NOTES

Prepared for the Sixth International Symposium on Unsteady Aerodynamics, Aeroacoustics, and Aeroelasticity of Turbomachines and Propellers sponsored by the International Union for Theoretical and Applied Mechanics, Notre Dame, Indiana, September 15–19, 1991. Daniel Hoyniak, NASA Lewis Research Center; Joseph M. Verdon, United Technologies Research Center, East Hartford, Connecticut 06108. Responsible person, Daniel Hoyniak, (216) 433–3789.

12a. DISTRIBUTION/AVAILABILITY STATEMENT

Unclassified - Unlimited
Subject Category 07

12b. DISTRIBUTION CODE

13. ABSTRACT ***(Maximum 200 words)***

A full potential steady flow solver (SFLOW) developed explicitly for use with an inviscid unsteady aerodynamic analysis (LINFLO) is described herein. The steady solver uses the nonconservative form of the nonlinear potential flow equations together with an implicit, least-squares, finite-difference approximation to solve for the steady flow field. The difference equations were developed on a composite mesh which consists of a C–grid embedded in a rectilinear (H–grid) cascade mesh. The composite mesh is capable of resolving blade-to-blade and far-field phenomena on the H–grid, while accurately resolving local phenomena on the C–grid. The resulting system of algebraic equations is arranged in matrix form using a sparse matrix package and solved by Newton's method. Steady and unsteady results are presented for two cascade configurations: a high-speed compressor and a turbine with high exit Mach number.

14. SUBJECT TERMS	15. NUMBER OF PAGES
Steady potential solver; Newton's method; Cascade; Sparce matrix solver	14
	16. PRICE CODE: A03

17. SECURITY CLASSIFICATION OF REPORT	18. SECURITY CLASSIFICATION OF THIS PAGE	19. SECURITY CLASSIFICATION OF ABSTRACT	20. LIMITATION OF ABSTRACT
Unclassified	Unclassified	Unclassified	